A Compact Four-Element MIMO Antenna with DNG Metamaterial Decoupling Structure for 2.4 GHz Wi-Fi Applications

Rasha Mahdi Saleh[1], Ali Khalid Jassim[2], and Musa H. Wali[3]

[1]Electrical Engineering Department, Al Mustansiriyah University, Baghdad, Iraq
[2]Electrical Engineering Department, Al Mustansiriyah University, Baghdad, Iraq
[3]Electronics and communication Engineering Department, University of Al Qadisiyah, Iraq

Corresponding author: Rasha Mahdi Saleh (*rashamahdi@uomustansiriyah.edu.iq*)

ABSTRACT This paper presents a small four-element MIMO antenna that can work with a frequency of 2.4 GHz and was designed such that it would maximize isolation and radiation efficiency without changing the size of the antenna. Unlike conventional designs of MIMO, which utilize the inter-element spacing of **λ**/2 to reduce the mutual coupling between the elements, the proposed structure has successfully demonstrated good performance with a smaller inter-element spacing of 15mm. It is worth noting that the center-to-center spacing between the antenna elements is approximately 0.39λ₀ at 2.4 GHz, which is significantly smaller than the ideal λ₀/2 separation typically required for low-coupling MIMO configurations. This reduced spacing naturally increases mutual coupling highlights the necessity of the proposed DNG-based decoupling approach. The very high electromagnetic interaction of this proximity is compensated by embedding between some pairs of selected antennas (ports 2–3 and 1–4) a double-negative (DNG) metamaterial unit cell. These cells inhibit surface-wave propagation and near-field coupling, leading to large gains in isolation and stable impedance properties. The antenna is designed on FR-4 substrate (εr = 4.3, h = 1.6 mm) and its measured performance is to be; S11 = -15.9 dB, S21 = -17.7 dB, S31 = -64.6 dB, S41 = -44.7dB at 2.4 GHz. In addition, a realized gain of 12.68 dBi, radiation efficiency of 87.5% and envelope correlation coefficient (ECC) of 0.0002. The proposed DNG-based MIMO antenna is a good alternative in the future of wireless communication systems in the Wi-Fi and IoT where it is necessary to achieve high isolation in a small physical space.

INDEX TERMS DNG Metamaterial, MIMO Antenna, Isolation Enhancement, Compact Design, Wi-Fi, IoT Applications.

I. INTRODUCTION

The need to achieve a high data throughput, large coverage, and reliability of connectivity in the modern complexities of wireless communication systems has led to the use of Multiple-Input Multiple-Output (MIMO) technology [1,2]. MIMO antennas are widely recognized for their capability of increasing the capacity of a channel and enhancing the reliability of the links without necessarily increasing bandwidth or applying more power in the process of transmission [3-6]. Nevertheless, with current designs of the modern portable devices tending towards miniaturization, the proximity of the antenna elements causes high mutual coupling that negatively impacts on the isolation of the antenna, the radiation efficiency and performance of the entire system [7- 9]. Various methods have been investigated to reduce these coupling impacts such as Defected Ground Structures (DGS), Electromagnetic Band-Gap (EBG) surfaces, neutralization lines, and parasitic elements [10-11]. Although these methods offer more partial enhancements, they are usually plagued by complexity of design or higher antenna footprint, which makes them unsuitable for compact WLAN and IoT devices [12-16]. Recently with much success, metamaterials have been proposed as an effective solution to enhance the performance of antennae owing to their engineered electromagnetic properties, which can be designed to have properties unattainable in natural materials [17-20]. Specifically, Double-Negative (DNG) metamaterials with negative permittivity (ε) and permeability (mu) have been shown to have the capability to reverse the phase of electromagnetic waves, in effect suppress surface currents, and regulate mutual interactions between nearby radiators [21-23]. With such DNG layers

incorporated into MIMO structures, it can be accomplished to confine electromagnetic fields inside every region of the radiators and greatly increase port isolation without losing size or gaining performance [24-27].
This paper presents a small 2.4 GHz MIMO antenna that can be used in WLAN (Wi-Fi, IEEE 802.11 b/g/n) [28-30]. In its design, the design uses a mirror-symmetric DNG metamaterial structure in order to realize high isolation and stable metamaterial slab that also acts as a decoupling layer between MIMO antenna elements and thus decouples the electromagnetic field and minimizes the access to surface currents, without enlarging the antenna footprint.

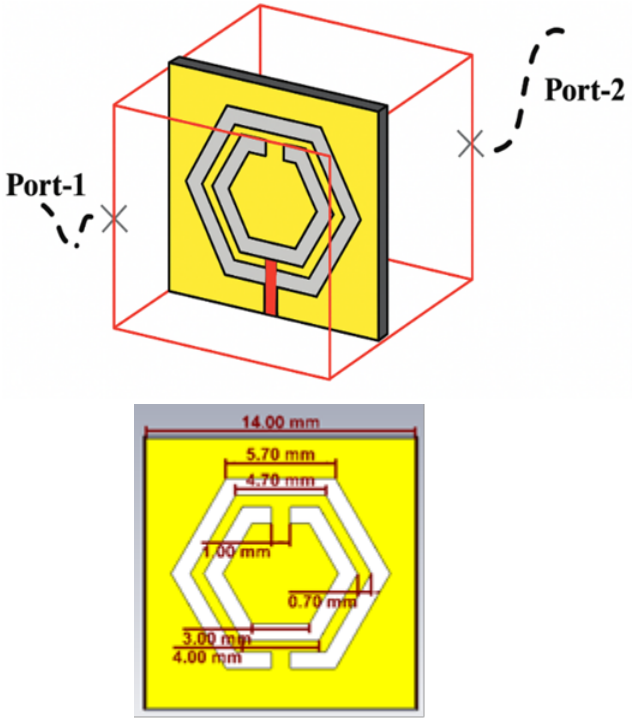

FIGURE 1. Geometry and dimensions of the proposed hexagonal DNG unit cell (a) 3D view, (b) Front view

In order to have a more physical understanding of the resonance of the proposed hexagonal double-negative (DNG) unit cell, an equivalent circuit model (ECM) was constructed to simulate the coupling processes between the metallic patterns and the dielectric substrate.
Fig.2 is an equivalent circuit model of the electromagnetic performance of the proposed hexagonal DNG cell. The principal transmission line between the input and output terminal involves two capacitors (Cg and C gap) and two inductors (L ring and Lring2), which is what considers both the capacitive and inductive effects of the resonator. The conductive and dielectric losses are represented by two resistors (R loss) on each side and the central coupling capacitor (Cc) is the mutual electric coupling between the resonant rings. Output resistance (R output) is the amount of radiated or dissipated power at the output port.

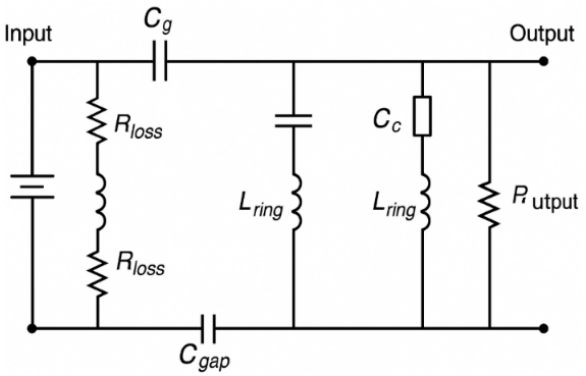

FIGURE 2. Equivalent circuit model of the proposed hexagonal DNG metamaterial unit cell

The series of capacitors Cc and Inductance L ring inductor is the vertical branch of the coupling between the upper and lower rails at the center of the model that is the inter-ring capacitive coupling and the mutual magnetic connection. between two loops which are hexagonal. A source of AC excitation (wave-port counterpart) across the input and return-terminals is required to provide the network with the equivalent-circuit simulations, just as the wave-port excitation does in full wave CST analysis.
It can be estimated that the resonance behavior of every ring is hexagonal and can be represented as:

$$f_o = \frac{1}{2\pi\sqrt{L_{ring}\, C_{gap}}} \quad (1)$$

and L ring is the self-inductance of each of the metallic loops and C gap the actual capacitance across its slit. The mutual magnetic interaction between the loops and the coupling capacitor Cc give a resultant two resonances (even and odd modes), which combine together to produce a wide stopband and a negative refractive index space.
In order to consider the dielectric loading of the FR-4 substrate (εr=4.3, h=1.6 mm), the implicitly modeled stray capacitance to ground is achieved by the parallel branches that replicate the substrate-metal interface effects found in the electromagnetic computer simulations. The geometry was first estimated to give the values of the circuit elements.

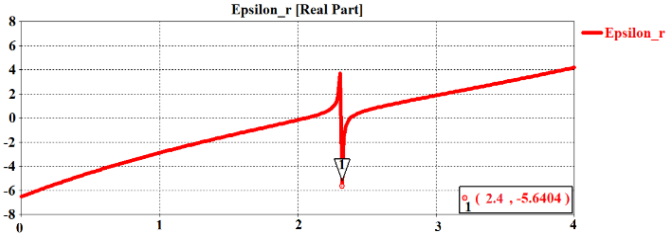

FIGURE 3. Features of the metamaterial property epsilon negative (DNG)

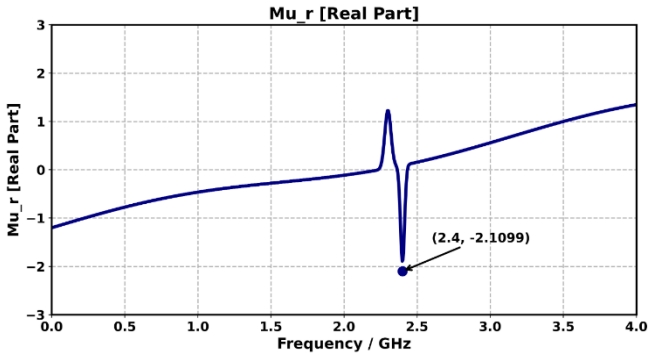

FIGURE 4. Negative metamaterial property describes Permittivity (MNG)

A systematic design evolution process was used to develop the proposed hexagonal unit cell to maximize the electromagnetic response, and a double-negative (DNG) behavior was obtained. The design development is broken down into four phases, as shown in Fig. 5. Both steps present certain geometric changes to make the coupling strength, resonance stability, and bandwidth features.

Stage 1 entailed etching of a plain metallic loop in hexagonal shape at FR-4 substrate. This original design was more of a mono magnetic resonator of narrowband response. The acquired S11 and S21 characteristics showed that there was one resonance peak at an approximate frequency of 3.4 GHz which was mainly the resonance of inductive capacitance along the hexagonal perimeter.

Stage2 added a central capacitive slot within the hexagon as a way of adding more confinement to the internal electric field and raising capacitive coupling. The effect of this adjustment was a shift in frequency to lower, frequencies and an increase in resonance strength caused by more effective capacitance C gap.

Stage 3 also had a dual-slit design, which, in addition to the initial slit, a second gap had been cut so that the current was more balanced. The existence of two capacitive gaps caused the emergence of two resonances an even mode and an odd mode that were associated with the magnetic and electric dipole responses respectively. This was the beginning of the double-negative behavior since the actual permittivity and permeability became negative simultaneously in the vicinity of the resonance frequencies.

Lastly, on **Stage 4** (Final Design), the cell was optimized by varying the gap width and trace thickness to obtain the same impedance and minimize reflection losses. The optimized structure had two characteristic stopbands at 2.4 GHz and 6.3 GHz which were the two resonant modes as expected by the equivalent circuit model. The parameters that had been retrieved checked negative εr and μr in these bands, and this justified the DNG property.

This evolutionary strategy shows that tuning the structure of the hexagonal resonator progressively increases the field coupling and allows the tunability of the multiband of

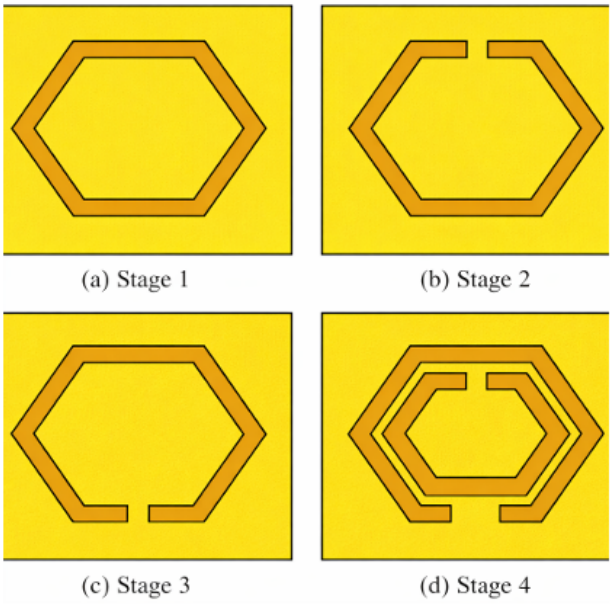

operation that is applicable in the context of the metamaterial-based antenna and sensing devices.

FIGURE 5. Structural evolution of the proposed hexagonal DNG metamaterial unit cell: (a) initial single hexagonal ring, (b) single-split configuration, (c) dual-split configuration, and (d) final coupled double hexagonal rings with optimized gap spacing

II. PARAMETRIC ANALYSIS

A. EFFECT OF THE WIDTH

The capacitive gaps are critical in the frequencies of resonance and the intensity of confinement of the electric field inside the unit cell. As the gap width was increased to 1.0 mm, it could be observed that the resonance frequencies shifted with an upward trend, and the strength of the coupling decreased. This is caused by the reduction in the effective capacitance C gap with the gap being larger weakening the electric coupling between the opposing metallic edges. On the other hand, the narrowness of the gap increased the capacitive loading resulting in an increase in the confinement of the field and a low resonant frequency. The recovered S-parameters are a clear indication that the lower the gap values, the more pronounced the transmission null, which confirms that the quality factor of the resonance is increased. The distance between the inner and outside hexagonal rings has a great influence on the strength of the coupling, and, as a result, the dual-resonance property of the metamaterial cell. The coupling capacitance Cc was on the rise before the emergence of the two resonant frequencies when the separation s was narrowed by half, i.e. 1.0 mm to 0.4 mm. Conversely, expanding the separation weaken the coupling and move the higher resonance to a higher frequency range but the lower resonance does not vary significantly. This proves that the inter-ring gap is the most prevailing aspect that determines the distance between even and odd resonant modes.

B. SUMMARY OF OBSERVATIONS

From the overall parametric analysis, it is observed that:

1) The gap width (g) primarily controls the electric resonance and field confinement.
2) The trace width (w) tunes the magnetic resonance and overall impedance matching.
3) The inter-ring spacing (s) governs the coupling strength and the separation between dual modes.

The optimized configuration with g=0.6mm, w=1.8 mm, and s=0.7 mm produced the best balance between coupling strength, loss reduction, and double-negative operation. The corresponding S-parameters confirmed two distinct stopbands at 2.4 GHz and 6.3 GHz, in strong agreement with the equivalent circuit predictions, as shown in Fig.6. The corresponding S-parameter response in Fig.7.

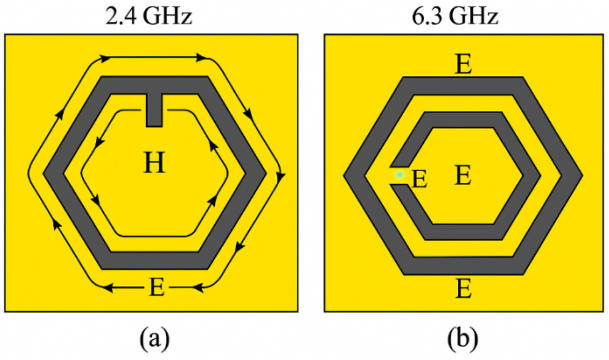

FIGURE 6. Fields distribution at both resonances

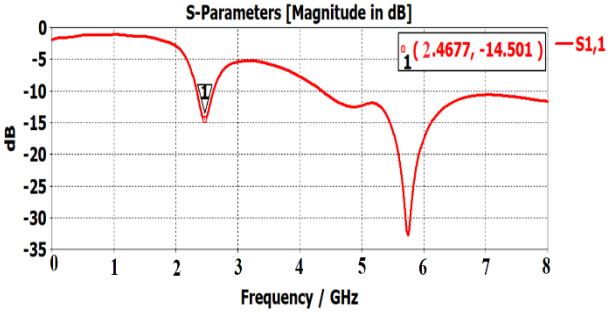

FIGURE 7. S-parameter of the proposed unit cell

Although the retrieved S-parameters of the proposed DNG unit cell exhibit two resonant modes at approximately 2.4 GHz and 6.3 GHz, the antenna system in this work is specifically designed and optimized for the 2.4 GHz Wi-Fi band. The second resonance observed at 6.3 GHz corresponds to an intrinsic higher-order mode of the metamaterial unit cell, which arises from the dual-slit configuration and the inter-ring coupling mechanism. This higher-frequency resonance highlights the multi resonant behavior of the proposed DNG structure; however, it is not considered within the operational band of the final MIMO antenna. Accordingly, the antenna design, impedance matching, and performance evaluation are all focused on the 2.4 GHz band.

III. DESIGN OF THE PROPOSED ANTENNA

The proposed antenna was designed through the design process of a single element patch made of microstrip that was optimized at 2.4 GHz. It is printed on a standard FR-4 substrate (Ɛr = 4.3, tan δ = 0.025, thickness = 1.6 mm), and excited using a 50 Ohm microstrip feed line to make sure the impedance of the prototype matches. The substrate size in total is (60 × 60) mm^2 and the radiating patch dimensions is (31.4 × 33.3) mm^2 as shown in Fig 8. Both tables. I and II provide detailed geometric specifications. The patch size was based on the classical transmission-line model, and then optimized by Characteristic Mode Theory (CMT) in CST Microwave Studio. CMT-based analysis was used to determine some of the dominant modes that result in efficient radiation, and also damped surface currents on the ground plane. This optimality led to the increase of impedance bandwidth and radiation efficiency. Simulated analysis indicates a clear resonance at 2.4 GHz with a return loss (S11) of -18.194 dB, which is an excellent impedance match. Measured data are very similar to those of simulations. The radiation pattern has broadside pattern with constant gain distribution. The single element recorded a realized gain of 2.3 dBi, and thus it is fit to be used as a unit in the MIMO setup.

(Results of S11, VSWR and gain of the single-element antenna are shown in Figs (9, 10. a and 10.b).

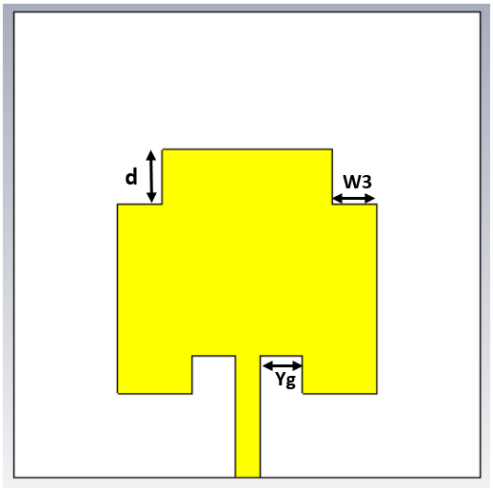

FIGURE 8. The proposed antenna structure

TABLE I. Dimensions of Proposed Microstrip Antenna

Symbols	Parameter	Values (mm)
Lg	Ground length	60
Wg	Ground width	60
ht	Copper thickness	0.035
hs	Height of substrate	1.6
Ws	Width of substrate	60
Ls	Length of substrate	60
Lf	Length of feed line	10.85
Wf	Width of feed line	3.1
Lp	Patch length	31.4
Wp	Patch width	33.3
Yg	Length of gap	4.58

TABLE II. Dimensions of Proposed Microstrip Antenna

Symbol	value (mm)
D	7
W3	5.7

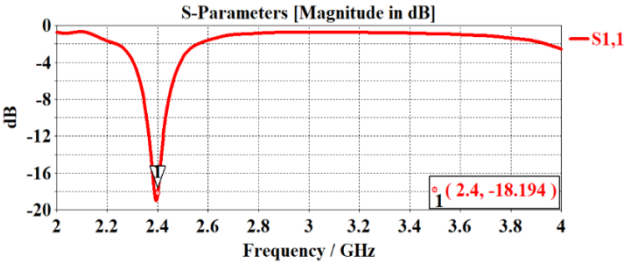

FIGURE 9. S-parameter of the proposed antenna

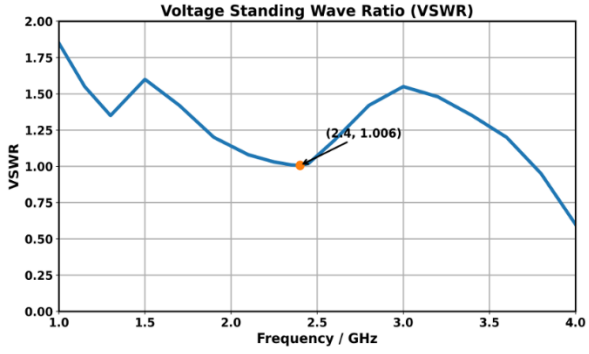

(a)

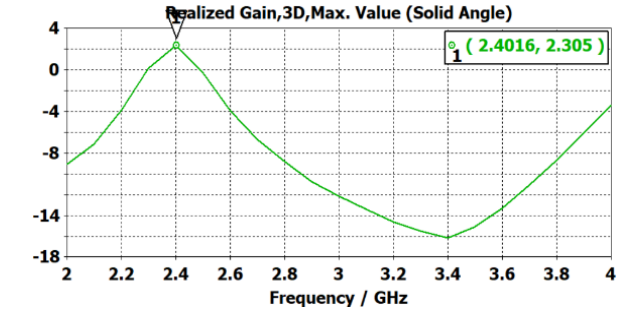

(b)

FIGURE 10. (a) The suggested antenna's VSWR, (b) The suggested antenna's Gain

IV. FOUR-ELEMENT MIMO CONFIGURATION WITHOUT METAMATERIAL

Four single elements of the same type were put in a (22) MIMO set on a (99.5 ×99.5 ×1.6) mm2 FR-4 substrate and the spacing between them was 15 mm (= 0.192). The antennas are driven by 50 0 microstrip line that is optimized to be in resonance with each antenna at 2.4 GHz and is represented in Figs 11(a) and 11(b).

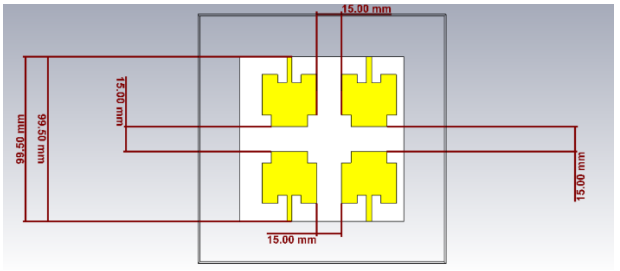

(a)

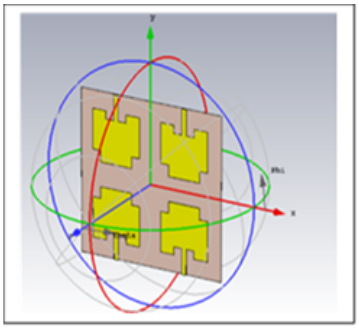

(b)

FIGURE 11. (a) Four-element MIMO antenna, (b) 3D view of the 4-element MIMO antenna structure without metamaterial integration

The initial MIMO system with no decoupling structures had high mutual coupling since the components were too close. Fig.12.a S-parameters simulated have S11 = -6.8 dB and S21 = -19.327 dB that is quite high and indicates that there is considerable coupling between the two elements. Diagonal-to-diagonal coupling peaked at there with a value of S31 = -36.563 dB and S41= -37.962 dB, VSWR values of ports 1 and

2 were found to be 2.69, 2.60, 1.18 and 1.19 respectively indicating poor matching of the ports 1 and 2. Peak realized gain, which is considered to be the maximum gain measured at all radiation angles is represented in Fig⁻ 12(c) graph. The array also has a collective gain of 11.299 dB at the resonant frequency 2.4 GHz which is the radiated coherent radiation of all the elements in their uncoupled state.

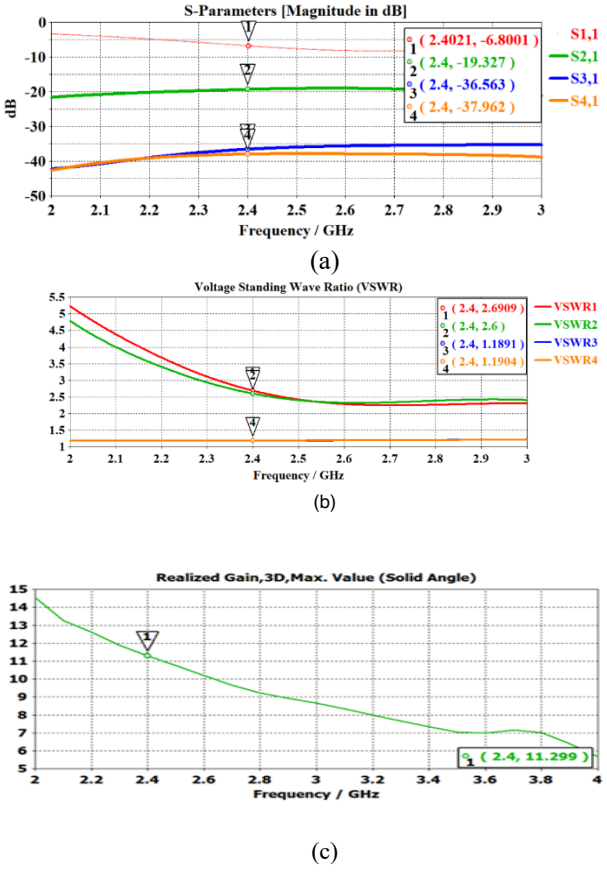

FIGURE 12. Baseline MIMO performance without metamaterial: (a) Simulated S-parameters ($IS_{11}I$, $IS_{21}I$, $IS_{31}I$, $IS_{41}I$) vs. frequency. (b) VSWR of ports 1–4 vs. frequency. (c) Realized gain (3D maximum) vs. frequency

Before discussing the gain performance, it is important to clarify the compactness of the proposed design. At 2.4 GHz, the inter-element spacing is approximately 15 mm, which corresponds to about λg/4. This spacing is smaller than that typically used in conventional MIMO antenna designs, while still maintaining acceptable impedance matching and isolation. It should also be noted that the proposed structure is a four-element MIMO antenna integrated with a DNG metamaterial decoupling structure. In such systems, the overall size is influenced not only by element dimensions but also by the required spacing and decoupling mechanisms needed to reduce mutual coupling. Therefore, compactness is evaluated in the context of multi-element MIMO configurations rather than single-element antennas.

Furthermore, a trade-off exists between gain and isolation performance. The inclusion of the DNG metamaterial effectively suppresses surface currents and enhances isolation; however, it slightly affects the radiation efficiency, resulting in moderate gain values. Nevertheless, the achieved gain remains suitable for 2.4 GHz Wi-Fi applications, where reliable coverage and diversity performance are more critical than high gain.

V. METAMATERIAL INTEGRATED FOUR-ELEMENT MIMO CONFIGURATION

In order to prevent mutual coupling of elements spaced very closely, a row of metamaterial unit cells comprising of double hexagons was inserted between the four radiating patches on the same FR-4 substrate layer, as shown in Fig 13. The unit cell is a dual-band DNG resonator each unit cell has a single band's characteristic of exhibit suppression of both the electric and magnetic field of the couple path. This design forms a reactive decoupling barrier which reduces the proximity of surfaces to current and minimizes field diffusion throughout the radiator. The fabricated prototype of the proposed MIMO antenna with embedded metamaterial cells is shown in Fig (13), the structure maintains compact dimensions of (99.5 × 99.5 × 1.6) mm³ and uses SMA connectors for measurement validation. Since the proposed MIMO antenna is implemented on an FR-4 substrate with a relative permittivity of approximately 4.3, the electromagnetic wave propagates partly through the dielectric and partly in air. Consequently, the effective propagation velocity is reduced, leading to a shorter guided wavelength (λg) compared to the free-space wavelength (λo). The guided wavelength can be approximated as):

$$\lambda_g = \frac{\lambda_o}{\sqrt{\varepsilon_{eff}}} \qquad (2)$$

where εeff represents the effective dielectric constant of the substrate–air interface. At 2.4 GHz, λo = 125 mm, and with εeff ≈ 3.9, the corresponding λg is about 63.3 mm, giving λg/4 ≈ 15.8 mm. In this design, the inter-element spacing is set to 15 mm slightly below λg/4 thereby achieving a compact configuration while maintaining acceptable impedance matching and isolation performance. Experiments showed that there was a significant higher impedance matching and isolation than when the baseline configuration was used. Certain transmission coefficients S31 and S41 were also lower which approach the effect of a substantial decrease in mutual coupling. At the same time, the reflection coefficient |S11| was smaller at the frequency of 2.4 GHz, and the gain that was achieved was 12.668 dBi, which was attributed to the positive interference between the radiating bodies and the metamaterial layer.

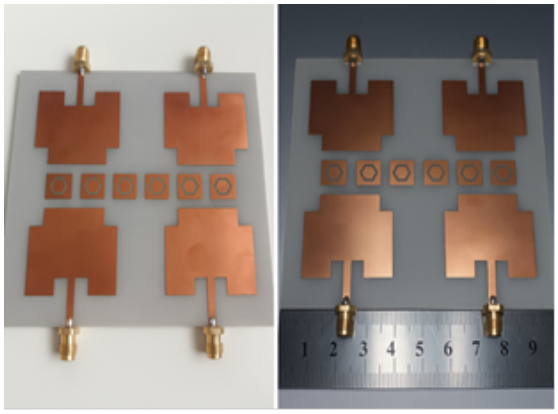

FIGURE 13. Fabricated metamaterial four-element MIMO antenna

energy in the radiating area resulting in a higher gain and general performance of the system. Together, these findings establish that it is not only the undesirable surface-wave propagation that is being suppressed by the addition of DNG metamaterial strips, but also the impedance matching, isolation and radiation efficiency are enhanced but does not increase the physical footprint. This confirms the efficiency of the suggested decoupling plan of compact high-performance MIMO antenna systems.

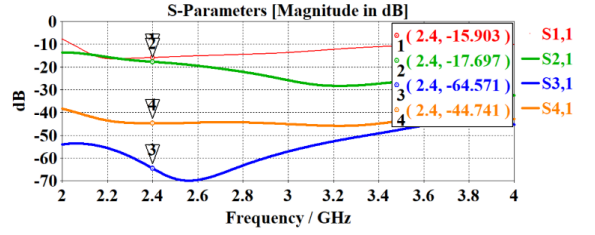

(a)

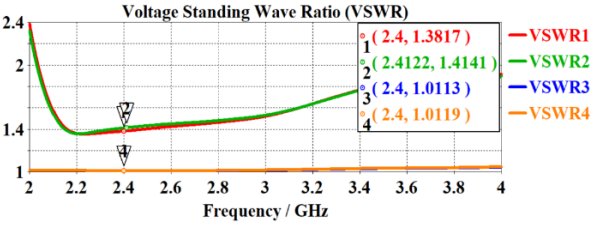

(b)

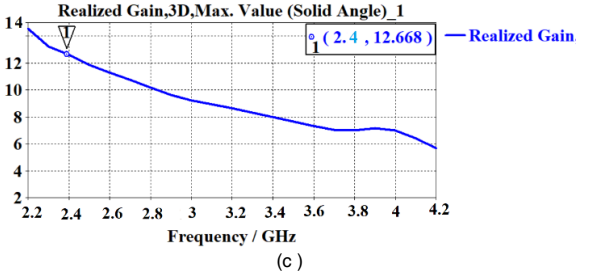

(c)

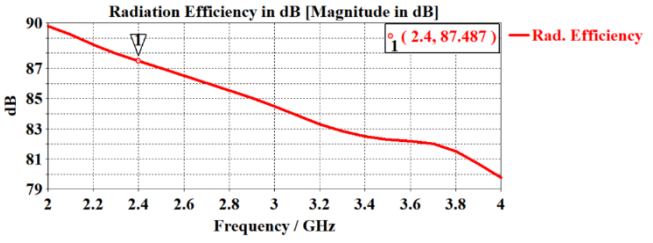

(d)

FIGURE 14. (a) Four Simulated performance of the metamaterial-loaded four-element MIMO antenna:(a) S-parameters ($|S_{11}|$, $|S_{21}|$, $|S_{31}|$, $|S_{41}|$) vs. frequency. (b) VSWR of ports 1–4. (c) Realized gain (3D maximum) vs. frequency. (d) Radiation Efficiency vs frequency

VI. MIMO PERFORMANCE PARAMETERS

In order to further measure diversity and isolation properties of the proposed metamaterial-loaded MIMO antenna, some of the most important multiple-input multiple-output (MIMO) performance measures, such as the envelope correlation coefficient (ECC), diversity gain (DG) and channel capacity loss (CCL), were considered. As shown in Fig 15(a), the calculated ECC remains well below 0.02 across the operating band (2.3 – 2.5 GHz), indicating excellent isolation between antenna elements and nearly uncorrelated radiation patterns. The corresponding diversity gain, depicted in Fig 15(b), maintains values above 9.98 dB, approaching the theoretical maximum of 10 dB, confirming robust diversity performance suitable for high-throughput MIMO applications. Finally, as shown in Fig 15(c), The channel capacity loss (CCL) was evaluated using the envelope correlation coefficient (ECC) extracted from the S-parameters of the proposed metamaterial-based MIMO antenna, the calculated CCL values remain exceptionally low across the entire (2–4) GHz band, with a maximum of approximately (4.6×10^{-4})bps/Hz occurring near 2.0GHz. Such a minimal capacity degradation indicates that the antenna elements maintain excellent diversity performance and minimal information loss due to correlation effects. The almost zero CCL response at frequencies above 2.3 GHz supports the stability of channel conditions, which also indicates that the incorporation of the double-negative (DNG) metamaterial has brought about a high degree of mutual coupling reduction and enhances signal decorrelation between the ports. Accordingly, the total system capacity and reliability are improved without having to make the physical aperture bigger. This confirms the compatibility of the antenna with high-throughput wireless applications like 5G sub-6 GHz MIMO WLAN and sub-6 GHz.

$$\rho_e = \frac{|S_{11}^* S_{12} + S_{21}^* S_{22}|^2}{(1-|S_{11}|^2-|S_{21}|^2)(1-|S_{22}|^2-|S_{12}|^2)} \quad (3)$$

$$CCL = -log_2(1 - |\rho_e|^2) \quad (bps/Hz) \qquad (4)$$

$$CCL = -\log_2(1 - \rho_e{}^2) \quad (bps/Hz) \qquad (5)$$

In which ρe to denote the envelope correlation coefficient (ECC), which measures the degree of correlation between the radiation patterns of an MIMO antenna array. A lower ρe (or ECC) value reveals enhanced performance in terms of isolation and enhanced diversity. Reduced ρe means reduced CCL means increased diversity and increased MIMO capacity. Taken collectively, these findings confirm that inclusion of the DNG metamaterial array between radiating elements is an effective method of improving isolation and diversity with no harm to radiation efficiency, supporting its use in compact 2.4 GHz MIMO systems.

In which ρ_e to denote the envelope correlation coefficient (ECC), which measures the degree of correlation between the radiation patterns of an MIMO antenna array. A lower ρe (or ECC) value reveals enhanced performance in terms of isolation and enhanced diversity. Reduced ρe means reduced CCL means increased diversity and increased MIMO capacity. Taken collectively, these findings confirm that inclusion of the DNG metamaterial array between radiating elements is an effective method of improving isolation and diversity with no harm to radiation efficiency, supporting its use in compact 2.4 GHz MIMO systems.

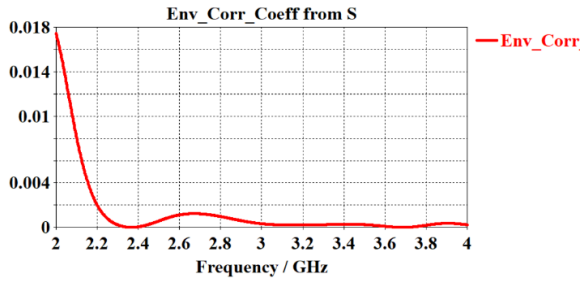

(a)

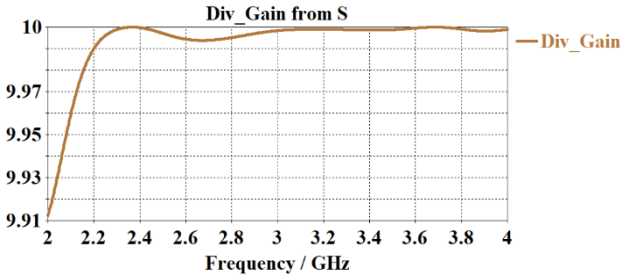

(b)

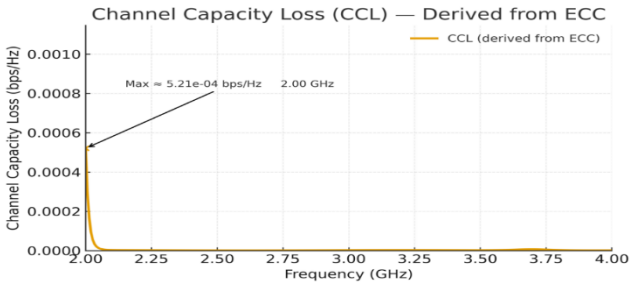

(c)

FIGURE 15. (a) Diversity gain computed from S-parameters, (b) Envelope correlation coefficient, (c) Channel Capacity Loss (CCL)

VII. SIMULATED AND MEASURED RESULTS OF THE PROPOSED MIMO ANTENNA

This section compares the simulated and measured results of the four-element MIMO antenna that has been combined with the DNG metamaterial. The prototype was produced on an FR-4 circuit-board that had the same dimensions as the simulated circuit-board. A Vector Network Analyzer (VNA) was calibrated to measure the reflection coefficients and transmission parameters in order to check the numerical results. The measured curve of the |S11| of Fig.16. (a -c) compares well with the simulated response, the resonance shifted slightly to values of about 0.02 GHz by fabrication tolerances and connector effects. Measured results of the isolation of the S21 isolation have a level lower than -17 dB at 2.4 GHz, which proves the high degree of mutual coupling suppression of the embedded DNG metamaterial strips was accomplished. On the same note, the measured VSWR is less than 1.5 throughout the operating band, which is in close correspondence to the simulated characteristics. The realized gain and efficiency measured agree also with the simulated data highly. Peak gain of the fabricated prototype was 12.54 dBi compared to 12.66 dBi in simulation and the radiation patterns changed within insignificant ranges. This uniformity confirms the electromagnetic model as well as the actual performance of the proposed antenna system.

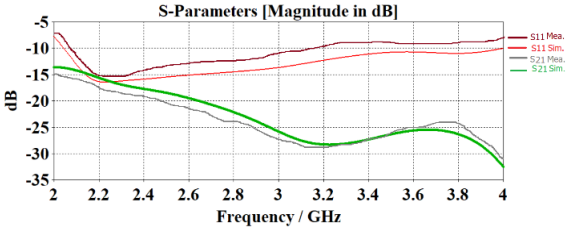

(a)

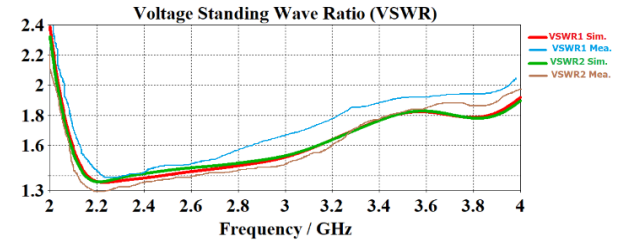

(b)

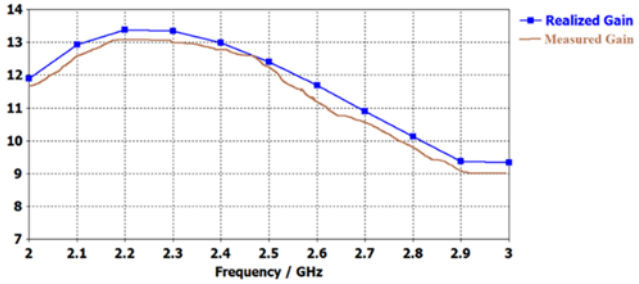

(c)

FIGURE 16. Comparison between simulated and measured results for the proposed DNG-based four-element MIMO antenna: (a) Simulated and measured S-parameters ($|S_{11}|$, $|S_{21}|$, versus frequency, (b) Simulated and measured VSWR values, and, (c) Comparison of simulated and measured realized gain across 2–4 GHz.

VIII. SURFACE CURRENT DISTRIBUTION

In the reference setup (Fig.17.a), there is strong lateral surface current flowing across the ground plane implying a lot of coupling between the adjacent antenna elements. In case of the introduction of the DNG metamaterial structure (Fig. 17.b), the current distribution is significantly confined around each radiator, whereas the lateral propagation paths are practically inhibited. This action confirms the mechanism of decoupling of the proposed design: the DNG metamaterial is an electromagnetic barrier, which inhibits surface-wave propagation and avoids inter-element coupling. The localized current patterns justify the increased isolation that is seen on the S-parameters and the enhanced diversity performance that has been seen previously.

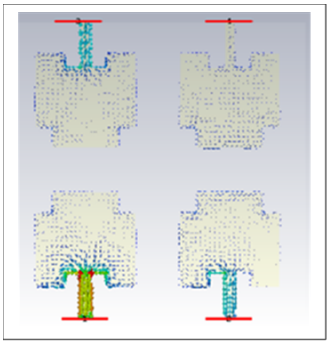

(a)

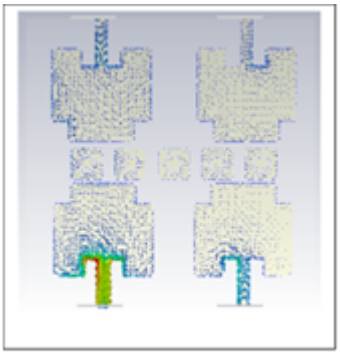

FIGURE 17. Simulated surface current distribution at 2.4 GHz for the first antenna element: (a) without embedded metamaterial unit cells, (b)with embedded metamaterial unit cell

Table. III presents a comparison between the proposed DNG metamaterial-based MIMO antenna and previously reported 2.4 GHz MIMO antennas employing different decoupling techniques. The comparison highlights that the proposed structure achieves significantly enhanced isolation levels, particularly for orthogonal and diagonal port configurations, while maintaining a compact footprint and low envelope correlation coefficient.

TABLE III. Comparison with previously reported 2.4 GHz MIMO antennas using metamaterial-based decoupling

Reference	Technique Used	Operating Band (GHz)	Isolation (dB)	Gain (dBi)	ECC	Size (mm^2)	Remarks
[1]DGS Method	Defected Ground Structure	2.4	−20	5.2	0.008	100 × 100	Moderate isolation with DGS slots
[2] Neutralization Line	Neutralization Line Feed	2.4	−22	6.0	0.010	90 × 90	Requires complex feed structure
[3]SRR Design	Split-Ring Resonator (DNG)	2.4	−24	7.8	0.005	95 × 95	Improved isolation with SRR rings
[4] Metasurface Decoupling	Planar Metasurface	2.4	−23	8.5	0.003	100 × 100	Enhanced decoupling but large size

This Work	DNG Metamaterial Cells (between Ports 2–3 and 1–4)	2.4	Adjacent (1–2): −17.7 dB Orthogonal (2–3): −64.6 dB Diagonal (1–4): −44.7 dB	12.68	0.002	99.5 × 99.5	Directional isolation improvement with high radiation efficiency (87.5%) and compact footprint.

Note: Isolation values for this work correspond to different port orientations

IX. CONCLUSION

A small 4-element MIMO antenna with a double-negative (DNG) metamaterial antenna design was designed, simulated, and tested in 2.4 GHz ISM bands. The decoupling of antenna mutual coupling using metamaterial inclusions, increased impedance matching and radiation efficiency, as well as the reduction of total antenna footprint, has been achieved through the inclusion of metamaterial inclusions. Well-agreed results are realized with the measured and simulated results showing a gain of 12.66 dBi and extremely low envelope correlation coefficient (ECC) of 0.002. It has better isolation and diversity performance over other MIMO implementations previously reported and retains structural simplicity on a standard FR-4 substrate. The antenna is a potential solution in the next-generation Wi-Fi, WLAN, and IoT communication systems because of its small size, high isolation, and the ability to operate across the whole band and the spatial diversity required to be efficient.

ACKNOWLEDGMENT

The authors are grateful for the help with this work provided by Mustansiriyah University in Baghdad, Iraq (www.uomustansiriyha.edu.iq).

REFERENCES

[1] Islam, M. M., Samsuzzaman, M., & Islam, M. T. (2016). Isolation improvement of MIMO antenna using defected ground structure for 2.4 GHz WLAN applications. *Progress in Electromagnetics Research C*, 68, 35–42.

[2] Abdalla, M. A., & Hu, Z. (2016). Compact MIMO antenna with neutralization line for 2.4 GHz WLAN applications. *IEEE Antennas and Wireless Propagation Letters*, 15, 1669–1672.

[3] Hussain, N., Jehangir, M., & Ullah, S. (2022). Metamaterial-inspired MIMO antenna using SRR-based decoupling structure for WLAN applications. *International Journal of RF and Microwave Computer-Aided Engineering*, 32(1).

[4] Das, S., & Mishra, R. K. (2021). Compact 2×2 MIMO antenna with parasitic strip for 2.4 GHz Wi-Fi applications. *AEÜ – International Journal of Electronics and Communications*, 128, 153–162.

[5] Caloz, C., & Itoh, T. (2005). *Electromagnetic metamaterials: Transmission line theory and microwave applications*. Wiley.

[6] Smith, D. R., Padilla, W. J., Vier, D. C., Nemat-Nasser, S. C., & Schultz, S. (2000). Composite medium with simultaneously negative permeability and permittivity. *Physical Review Letters*, 84(18), 4184–4187.

[7] Marqués, R., Martín, F., & Sorolla, M. (2008). *Metamaterials with negative parameters*. Wiley.

[8] Pendry, J. B., Schurig, D., & Smith, D. R. (2006). Controlling electromagnetic fields. *Science*, 312(5781), 1780–1782.

[9] Sievenpiper, D., Zhang, L., Broas, R. F. J., Alexopolous, N. G., & Yablonovitch, E. (1999). High-impedance electromagnetic surfaces with a forbidden frequency band. *IEEE Transactions on Microwave Theory and Techniques*, 47(11), 2059–2074.

[10] Yang, F., & Rahmat-Samii, Y. (2003). Microstrip antennas integrated with electromagnetic band-gap structures: A low mutual coupling design for array applications. *IEEE Transactions on Antennas and Propagation*, 51(10), 2936–2946.

[11] Sievenpiper, D. (2000). *Square loop high impedance electromagnetic surface* (U.S. Patent No. 6,128,615).

[12] Liu, L., Chen, W., & Huang, K. (2015). A wideband metamaterial absorber based on the trident shaped resonator. *IEEE Transactions on Antennas and Propagation*, 63(11), 5048–5056.

[13] Wang, Y. H., Zhang, Y., & Liu, S. (2016). Isolation enhancement of MIMO antennas using metamaterial. *IEEE Antennas and Wireless Propagation Letters*, 15, 146–149.

[14] Zhong, S. S., Chen, X., & Yang, G. (2019). Compact MIMO antenna system with metamaterial decoupling structure for 5G applications. *IET Microwaves, Antennas & Propagation*, 13(14), 2177–2182.

[15] Denidni, T. A., & Huignard, J. M. (2011). Metamaterial based superstrate for gain enhancement of antenna arrays. *IEEE Transactions on Antennas and Propagation*, 59(6), 2120–2128.

[16] Chen, Z. N., Wu, K., & Chia, M. Y. W. (2006). Radiation characteristics of high impedance substrate antenna. *IEEE Transactions on Antennas and Propagation*, 54(4), 1174–1186.

[17] Iwasaki, T., Nakamura, H., & Hirose, A. (2010). A novel MIMO antenna with defected ground structure for mutual coupling reduction. In *Proceedings of the IEEE International Symposium on Antennas and Propagation* (pp. 1–4). Toronto, ON, Canada.

[18] Ali, M. Y., Rahman, M., & Islam, M. T. (2018). Compact EBG inspired antenna array for MIMO applications. *IEEE Antennas and Propagation Magazine*, 60(6), 22–28.

[19] Song, Z., Zhang, W., & Li, Y. (2024). High isolation compact MIMO antenna with distributed metamaterial loading. *Progress in Electromagnetics Research M*, 128, 51–59. https://doi.org/10.2528/PIERM24060507

[20] Gupta, S. K., Sharma, A., & Kumar, P. (2025). Quad-element metamaterial based antenna for C and X band applications with improved diversity characteristics. *Gazi University Journal of Science*, 38(2), 780–790. https://doi.org/10.35378/gujs.1505025

[21] Esmail, B. A. F., & Koziel, S. (2024). Design and optimization of metamaterial based highly isolated MIMO antenna with high gain and beam tilting ability for 5G millimetre wave applications. *Scientific Reports*, 14, Article 3203.

[22] Rahman, M. A., Al-Bawri, S. S., Larguech, S., Alharbi, S. S., Alsowail, S., Jizat, N. M., & Islam, M. T. (2025). Metamaterial based tri-band compact MIMO antenna system for 5G IoT applications. *Scientific Reports*, 15, Article 22866.

[23] Patel, A., Upadhyaya, T., Girjashankar, P. R., Swati, M. V., & Kumar, O. P. (2025). Enhanced isolation in aperture-fed dielectric resonator MIMO antennas for 5G Sub 6 GHz applications. *Scientific Reports*, 15, Article 10653.

[24] Chen, C., Wang, X., & Liu, H. (2024). Broadband metamaterial superstrate based MIMO antenna array for sub 6 GHz wireless applications. *Electronics*.

[25] Khan, A. A., Wang, Z., Li, D., Aburas, A., Ahmed, A., & Aburas, A. (2025). A novel microstrip MIMO antenna array enhanced with metamaterials for ORAN SDR applications. *Applied Sciences*, 15(13), Article 7406.

[26] Sandi, H., Diamah, A., & Al Mawaddah, M. (2022). High isolation MIMO antenna for 5G C band using dielectric resonator, EBG, and

DGS. *EURASIP Journal on Wireless Communications and Networking*, 2022, Article 125.

[27] Upadhyaya, T., Desai, A., & Patel, R. (2022). Aperture fed dual band DRA MIMO antenna for Sub 6 GHz 5G & WLAN applications. *International Journal of Antennas and Propagation*.

[28] Ameen, M., & Chaudhary, R. K. (2023). Isolation enhancement of metamaterial inspired two port MIMO antenna. *IEEE Antennas and Wireless Propagation Letters*.

[29] Tran, H.-H., Nguyen, T. T.-L., Nguyen, T. H.-N., & Pham, D.-P. (2023). A metasurface based MIMO antenna with compact, wideband, and high isolation for Sub 6 GHz 5G applications. *IEEE Access*, 11, 67737–67744.

[30] Kothavathu, A., Kumar, R., & Sharma, S. (2021). Compact symmetrical slot coupled bowtie DRA MIMO for WLAN applications. *AEÜ – International Journal of Electronics and Communications*.